THE JOURNAL OF PHYSICAL CHEMISTRY C
A JOURNAL OF THE AMERICAN CHEMICAL SOCIETY

pubs.acs.org/JPCC

Article

Probing Electrolyte Influence on CO_2 Reduction in Aprotic Solvents

Reginaldo J. Gomes, Chris Birch, Morgan M. Cencer, Chenyang Li, Seoung-Bum Son, Ira D. Bloom, Rajeev S. Assary, and Chibueze V. Amanchukwu*

Cite This: *J. Phys. Chem. C* 2022, 126, 13595−13606

Read Online

ACCESS | Metrics & More | Article Recommendations | Supporting Information

ABSTRACT: Selective CO_2 capture and electrochemical conversion are important tools in the fight against climate change. Industrially, CO_2 is captured using a variety of aprotic solvents due to their high CO_2 solubility. However, most research efforts on electrochemical CO_2 conversion use aqueous media and are plagued by competing hydrogen evolution reaction (HER) from water breakdown. Fortunately, aprotic solvents can circumvent HER, making it important to develop strategies that enable integrated CO_2 capture and conversion. However, the influence of ion solvation and solvent selection within nonaqueous electrolytes for efficient and selective CO_2 reduction is unclear. In this work, we show that the bulk solvation behavior within the nonaqueous electrolyte can control the CO_2 reduction reaction and product distribution occurring at the catalyst−electrolyte interface. We study different tetrabutylammonium (TBA) salts in two electrolyte systems with glyme ethers (e.g., 1,2 dimethoxyethane or DME) and dimethyl sulfoxide (DMSO) as a low and high dielectric constant medium, respectively. Using spectroscopic tools, we quantify the fraction of ion pairs that forms within the electrolyte. Also, we show how ion pair formation is prevalent in DME and is dependent on the anion type. More importantly, we show that as ion pair formation decreases within the electrolyte, CO_2 current densities increase, and a higher CO Faradaic efficiency is observed at low overpotentials. Meanwhile, in an electrolyte medium where the ion pair fraction does not change with the anion type (such as in DMSO), a smaller influence of solvation is observed on CO_2 current densities and product distribution. By directly coupling bulk solvation to interfacial reactions and product distribution, we showcase the importance and utility of controlling the reaction microenvironment in tuning the electrocatalytic reaction pathways. Insights gained from this work will enable novel electrolyte designs for efficient and selective CO_2 conversion to desired fuels and chemicals.

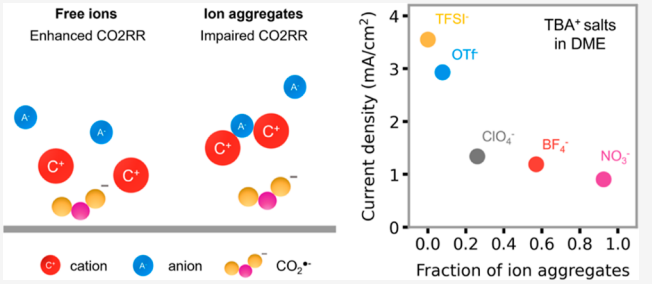

INTRODUCTION

Lower renewable electricity costs and continued emission of greenhouse gases have spurred the electrochemical reduction of carbon dioxide (CO_2) as a viable option for fuels and chemical production.[1−4] Currently, the most prevalent approach for CO_2 electrochemical reduction reaction (CO_2RR) consists of CO_2 heterogeneous catalysis over a metallic electrode. This approach has yielded a myriad of CO_2RR products, spanning from carbon monoxide to multicarbon/multihydrogenated products, such as ethylene, ethanol, and *n*-butanol.[5−7] However, CO_2RR in an aqueous medium is always plagued by the competing hydrogen evolution reaction (HER),[8,9] which occurs at similar electrochemical potentials. Moreover, CO_2 mass transport is often limited by poor CO_2 solubility in water and the competing equilibrium between CO_2 and carbonate species at medium to high pH.[10,11]

One strategy to circumvent the competing HER is to use solvents other than water.[12] Organic solvents such as acetonitrile (ACN), dimethylformamide (DMF), and dimethyl sulfoxide (DMSO) can suppress HER because they do not have any easily ionizable protons that could be further reduced. When combined with either organic salts or ionic liquids, these aprotic solvents have enabled faradaic efficiency (FE) values above 90% for carbon monoxide,[13,14] formic acid,[15,16] and oxalic acid.[17] Moreover, CO_2 mass transport can be facilitated in these solvents due to their high CO_2 solubility when compared to water.[15,18,19] Aprotic solvents have also been used industrially for CO_2 physical absorption, such as dimethyl ethers of polyethylene glycol (Selexol or Coastal AGR), *N*-methyl-2-pyrrolidone (Purisol), and propylene carbonate (Fluor Solvent).[20,21] Therefore, the use of an aprotic solvent for CO_2RR could leverage the development of new technologies that integrate both CO_2 capture and conversion.

In addition to solvent effects, the nature of the supporting electrolyte also plays an important role in the CO_2RR current density and selectivity. For an aqueous medium, it has been

Received: May 13, 2022
Revised: July 13, 2022
Published: August 4, 2022

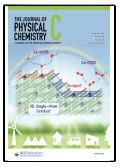

Scheme 1. Chemical Structures of the Herein Investigated Solvents and Salts. Compounds are 1,2 Dimethoxyethane (DME), Diglyme (DGME), Tetraglyme (TGME), Dimethyl Sulfoxide (DMSO), Tetrabutylammonium (TBA^+), Perchlorate (ClO_4^-), Nitrate (NO_3^-), Bistriflimide ($TFSI^-$), Triflate (OTf), and Tetrafluoroborate (BF_4^-)

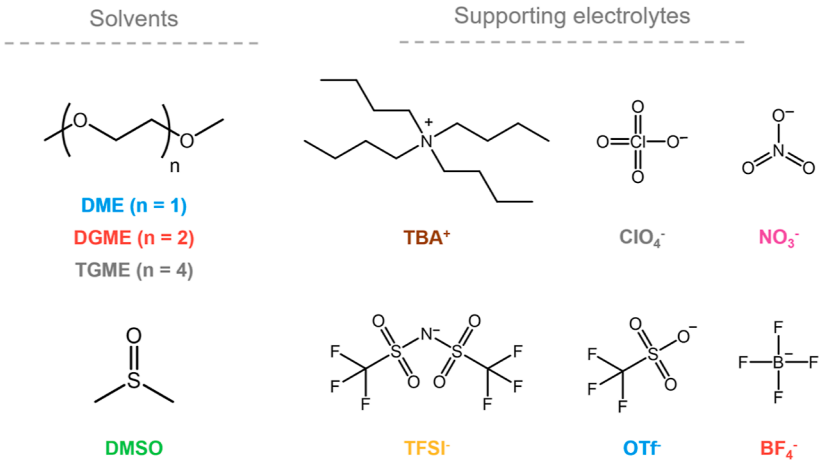

widely reported that large alkaline cations (such as Cs^+) can enhance CO_2RR current densities and the formation of multicarbon products by stabilizing the high dipole intermediates at the electrode surface through short- and medium-range interactions.[22−24] On the other hand, the identity and concentration of the anion can influence the CO_2RR selectivity by either buffering the local pH or acting as a proton donor.[25,26] Halides can also react with the copper electrode surface and facilitate the coupling of adsorbed CO molecules that results in a larger production of ethanol and ethylene.[27,28] However, the role of the electrolyte (salt and solvent) in the CO_2RR performance in an aprotic medium is still controversial. Voltammetric studies conducted in DMF with quaternary ammonium salts have shown that the nature of either the cation or the anion has little or no effect on the CO_2RR current density.[29,30] In contrast, studies conducted in ACN with tetraethylammonium salts have shown that switching the counterion from BF_4^- to triflate (OTf^-) results in a significant increase in current densities, which was only attributed to differences in the solution water content.[31] Moreover, the nature of the anionic species also played an important role in dictating the product distribution toward either formic acid or HER in ACN/ionic liquid/water mixtures.[16]

Recent studies on $Li-O_2$[32,33] and $Na-O_2$ batteries[34] have shown that electrolyte solvation can be modulated to control the oxygen reduction reaction (ORR) pathway. Therefore, the differences in the CO_2RR electrochemical performance in aprotic solvents might also be dictated by the electrolyte solvation behavior. For example, in $Li-O_2$ batteries, low donor number solvents such as glyme ethers lead to a surface-driven ORR pathway due to poor superoxide (O_2^-) solubility, while high donor number solvents such as DMSO with high O_2^- solubility lead to a solution-driven ORR pathway.[35] Differences in electrolyte solvation, and thereby transport and electrochemical properties, are more accentuated when using a low-coordinating solvent. For instance, solvation in weakly coordinating glyme ethers presents a strong dependence on the anion basicity[34] and solvent chain length.[36] In contrast, the nature of the anion presents a weaker effect on electrolyte solvation,[34] ion mobility,[37] and oxygen activity[38] in the highly coordinating DMSO.

In this work, we investigated the solvation effects on the CO_2RR performance in aprotic solvents. We selected two widely different solvents, 1,2-dimethoxyethane (DME) and DMSO, to further correlate bulk solvation properties to electrochemistry performance. Surprisingly, there are no studies reported on the use of any glyme ethers in CO_2RR, despite their large electrochemical window, high CO_2 solubility, and industrial relevance for CO_2 capture. We show that the CO_2RR current density correlates with the ether chain length, solvent choice (DMSO vs DME), tetrabutylammonium (TBA) salt concentration, and the salt anion (solvent and salt structures investigated herein are illustrated in Scheme 1). We quantify the influence of salt on the solvation behavior in DME- and DMSO-based electrolytes and show that a higher fraction of ion aggregates in DME-based electrolytes leads to lower current densities, where the anion identity controls the propensity for aggregate formation. In contrast, across the TBA salts studied in DMSO, a lower fraction of aggregates was observed, and these anions had little influence on the observed CO_2RR current density. Using Cu as the electrocatalyst, electrolytes with a low population of ion pairs yielded larger FE values for CO at lower overpotentials, while a high population of ion pairs led to high FE values for hydrogen across different potentials. By coupling bulk solvation to interfacial reactions and product distribution, we broadened our understanding of how the electrolyte microenvironment could affect the CO_2RR performance in aprotic systems. Insights gained from this work will facilitate the design of more efficient and selective electrolytes for integrated CO_2 capture and conversion to desired fuels and chemicals.

EXPERIMENTAL SECTION

Materials. Sodium perchlorate (98%), sodium hydroxide (99.99%), barium hydroxide octahydrate (98%), dimethoxyethane (anhydrous, 99.5%, inhibitor-free), diglyme (anhydrous, 99.5%), tetraglyme (anhydrous, 99%), dimethyl sulfoxide (anhydrous, 99.9%), 4 Å molecular sieves, decamethylferrocene (97%), tetrabutylammonium bistrifluoromethanesulfonimidate (99%), tetrabutylammonium tetrafluoroborate (99%), and tetrabutylammonium hydroxide ($TBAOH·30H_2O$, 98%) were purchased from Sigma-Aldrich. Nafion N-117 membrane (0.18 mm thick, >0.9 meq/g

https://doi.org/10.1021/acs.jpcc.2c03321
J. Phys. Chem. C 2022, 126, 13595−13606

exchange capacity), tetrabutylammonium triflate (99%), perchlorate (99%), and nitrate (99%) were purchased from Alfa-Aesar. Deuterated ACN (≥99.8 atom % D) and deuterated DMSO (≥99.8 atom % D) were purchased from Cambridge Isotope Laboratories. All solvents used for preparing electrolyte solutions were dried by 4 Å molecular sieves overnight (and stored with molecular sieves) inside an argon-filled glovebox (VigorTech, O_2 and H_2O < 1 ppm). All salts used in electrochemical experiments were vacuum-dried at 90 °C overnight in a heated glovebox antechamber before use and were not exposed to air at any time. Other chemicals were used as received. The copper electrode was assembled by fitting the superconductive copper rods (31.65 mm^2, 99.99%) into a PTFE tube, both purchased from McMaster-Carr. Platinum foils (99.99%) were acquired from BeanTown Chemical, while gold disk electrodes (7.07 mm^2) and leakless miniature Ag/AgCl electrodes were purchased from eDAQ. Carbon dioxide gas (99.9995%) and argon gas (99.999%) were purchased from Airgas.

Electrochemical Experiments. The voltammetric experiments were performed using a three-electrode configuration in a beaker cell (Figure S1a) at room temperature inside an argon-filled glovebox. A platinum foil was used as a counter electrode and a leakless miniature Ag/AgCl as a reference electrode. Before each experiment, the working electrodes (Cu and Au) were soaked in a 0.1 M aqueous phosphoric acid solution for 1 h, then polished with alumina suspension, rinsed with Milli-Q water (18.4 MΩ cm), and sonicated for 10 min. The electrochemical potential was controlled using a Biologic VSP-300 potentiostat and compensated for 85% of the value of R_u. The electrolyte solutions were purged with argon and CO_2 for 5 min for an experiment under argon and CO_2 atmosphere, respectively. The value of the decamethylferrocene redox potential was first accessed using cyclic voltammetry measurements in a separate electrolyte solution containing 2 mM Fc* to convert Ag/Ag^+ to the Fc* scale. As we observed that DMSO decomposes at more positive potentials for a copper electrode, conversions to the Fc* scale were made using a gold electrode for the same electrolyte.

Product Distribution Analysis. The CO_2RR product distribution was investigated using an H-cell setup (Figure S1b) inside the argon-filled glovebox, where the platinum foil was used as a counter electrode, a leakless Ag/AgCl as a reference electrode, and copper rod as a working electrode. The catholyte compartment was filled with the electrolyte sample, while a solution containing 0.5 M $TBAClO_4$ and 0.5 M water in the solvent of interest was used as an anolyte. Both chambers were separated by a Nafion-N117 proton exchange membrane. The catholyte was stirred at 1000 rpm, while a constant CO_2 flow of 10 sccm was fed into the solution. The CO_2 inlet tubing was placed in such a way that the gas bubbles did not hit the cathode surface. Products in the gas phase were analyzed using a Shimadzu GC-2014 gas chromatograph with both a flame ionization detector (FID) and a thermal conductive detector (TCD). Products in the liquid phase were quantified using ^{1}H NMR in a Bruker Ascend 9.4 T/400 MHz instrument. The analytical curve used for the quantification of formic acid is shown in Figure S2. The methods and equations used for the calculation of the product distribution are further described in the Supporting Information.

NMR Spectroscopy for Solvation Studies. All NMR samples were prepared inside an argon-filled glovebox using a coaxial capillary setup, where the electrolyte is placed inside a capillary tube (New Era Enterprises) and sealed with a PTFE cap from the surrounding deuterated solvent (D-acetonitrile).[39,40] The deuterated solvent was placed inside an NMR tube (Wilmad), which was then capped and sealed with Parafilm before analysis on a Bruker Ascend 9.4 T/400 MHz instrument. The ^{1}H chemical shift values were referenced to the residual nondeuterated ACN (1.93 ppm). As the NMR signal for the DME solvent hindered the signal from hydrogen in the alpha position (α-H) in the TBA cation, the chemical shifts for α-1H were determined using a 2D homonuclear correlation spectroscopy (COSY) experiment.

ESI-MS Studies. All samples were prepared inside the argon-filled glovebox and stored in 2 mL autosampler vials (ThermoFisher Scientific) to avoid major exposure to oxygen, which can accelerate the glyme ether decomposition.[41,42] The samples were analyzed using an Agilent Technologies 1260 Infinity chromatograph equipped with an electrospray, quadrupole mass spectrometer detector (Agilent Technologies 6120; MSD). The fragmenting voltage in the MSD was 70 V, and data were collected in the m/z range of 50−1000. Typically, 2−5 mL was directly injected into the MSD using a Hamilton syringe by hand. The mass spectral data were collected as full Gaussians. The mass spectral data were analyzed with the methods of Malinowski.[43] Here, single-ion chromatograms were used to calculate the mass spectra, as described in other works.[44,45]

XPS Characterization. Copper foils were cut into strips (1 cm × 4 cm) and used as a working electrode in a three-electrode setup, with Ag/AgCl as a reference electrode and platinum foil as a counter electrode. Electrolysis was performed inside an argon-filled glovebox. The copper foils were not stored inside the glovebox to avoid contamination, and they were used as received. After electrolysis, all the copper foils were rinsed three times with DME and dried for 1 h at room temperature outside the glovebox. XPS experiments illustrated in Figure 1b and Figures S3 and S4 were performed on a Kratos Axis Nova spectrometer. Experiments in Figure 1c,d were performed using a PHI 5000 VersaProbe II system (Physical Electronics). The spectra were obtained using an Al Ka radiation ($h\nu$ = 1486.6 eV) beam (100 μm, 25 W), Ar^+ and electron beam sample neutralization, in Fixed Analyzer Transmission mode. The XPS spectra were aligned to the C−C component in the C 1s spectra at 284.8 eV. Peak fitting was performed using Shirley background correction and the Gaussian−Lorentzian curve synthesis available in CasaXPS software.[46]

RESULTS AND DISCUSSION

Carbon Dioxide Reduction in Glyme Ether Solvents. Glyme ethers have been explored for a variety of electrochemical systems, ranging from electrochemical double-layer capacitors[47] to battery chemistries such as lithium metal,[48] sodium-ion,[49] and nonaqueous redox flow batteries.[50] Their widespread use is attributed to the propensity to dissolve and coordinate alkali and alkali earth cations, high reductive stability, and low viscosities. On the other hand, alkali cations have been the dominant supporting ions within the electrolyte for aqueous CO_2RR, as they can enhance the reaction selectivity toward value-added products such as ethylene and ethanol.[51,52] A recent study has also shown that multivalent cations could have an even larger enhancing effect on CO_2 reduction if water reduction could be hindered.[53] Accessing

https://doi.org/10.1021/acs.jpcc.2c03321
J. Phys. Chem. C 2022, 126, 13595−13606

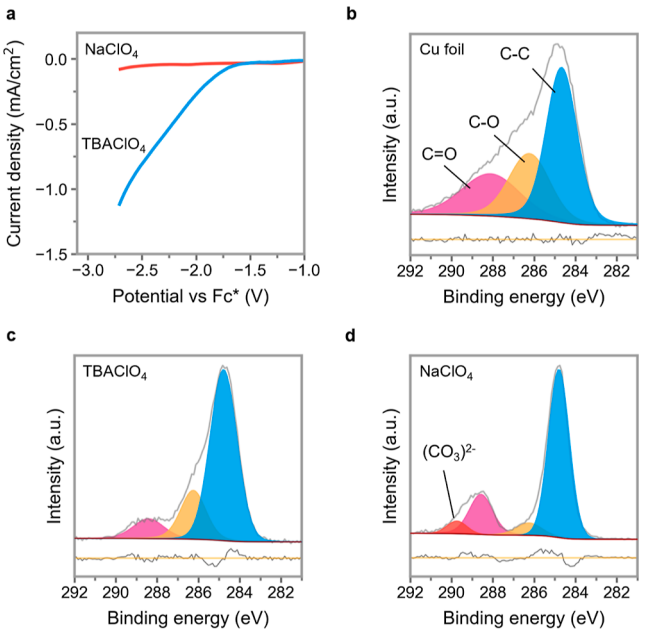

Figure 1. Influence of cation selection. (**a**) Linear sweep voltammograms (LSVs) for Cu electrode at 50 mV/s in CO_2 atmosphere in the presence of 0.5 M $NaClO_4$ and 0.5 M $TBAClO_4$ in DME. High-resolution XPS C 1s spectra of the metallic copper catalyst (**b**) before CO_2RR, after 10 min electrolysis at −2.6 V vs Fc* in DME with electrolytes containing (**c**) $TBAClO_4$ and (**d**) $NaClO_4$ salts.

highly reductive potentials in combination with appropriate cation selection may enable further reduced products. However, in aqueous systems, hydrogen evolution outcompetes CO_2RR at highly reductive potentials where further reduced products may be expected.[54−56] Therefore, we hypothesized that combining alkali cations with reductively stable glyme ethers may enable selective CO_2RR.

Linear sweep voltammetry (LSV) was performed to understand the effect of salt selection for CO_2RR in aprotic electrolytes. Figure 1a shows the voltammograms of a copper electrode in a DME electrolyte containing dissolved TBA and sodium salts. Potential measurements were standardized to the decamethylferrocenium/decamethylferrocene (Fc*) redox potential as other authors[29] have indicated that the nature of the electrolyte can affect the silver wire reference electrode potential. In addition, decamethylferrocene has been reported as more stable compared to ferrocene, especially in the presence of radical anions such as superoxides,[57,58] and we anticipate similar concerns in the presence of the carbon dioxide radical anion intermediate. Unfortunately, as Figure 1a shows, the presence of sodium ions appears to inhibit CO_2RR at reductive potentials up to −2.8 V (vs Fc^{*+}/Fc*). This phenomenon has also been observed by previous authors with different aprotic solvents, such as ACN[31] and DMF.[29] Nevertheless, when $NaClO_4$ salt is replaced by $TBAClO_4$, CO_2RR can be confirmed by an increase in current at a potential around −1.8 V. To the best of our knowledge, this is the first report of electrocatalytic CO_2 reduction in a glyme ether solvent.

Previous works[31,59] have suggested that CO_2RR in nonaqueous electrolytes containing alkali cations (M^+) can be deactivated by the competitive reduction of M^+ to M^0. However, the potentials for Na^+ or Li^+ reduction are more negative (around −3.0 V vs Fc*; see Figure S5) than the potentials needed for CO_2RR. Furthermore, the alkali cation reduction hypothesis is not sufficient to explain the complete inhibition of CO_2RR, as electrodeposition will lead to a reductive current signal.[39,41] To further probe the effect of alkali cation on suppressing CO_2RR, we performed X-ray photoelectron spectroscopy (XPS) on the copper electrode before and after electrolysis in the presence of CO_2. The C 1s XPS data in Figure 1b,c for pristine Cu foils before and after electrolysis in TBA-containing electrolytes show no modification of the catalyst surface. However, when an alkali cation is present, a layer of inorganic carbonate species is formed on the catalyst surface (Figure 1d). Unlike aqueous electrolytes, these alkali carbonates and bicarbonates are insoluble in glyme ethers, acting as an insulating layer that prevents any further electrochemical reaction on the electrode surface, including the facile Fc^{*+}/Fc* reversible reference reaction (Figure S6). Similar decay in electrochemical performance has also been observed in metal-CO_2 batteries, where the formation of alkali carbonates in an aprotic medium results in poor rechargeability.[60,61] Different authors have proposed that carbonates and bicarbonates can be generated in situ during the CO_2RR. For a dry electrolyte, carbonates can be formed by the reaction and disproportionation of two CO_2 molecules.[62,63] When water is present, carbonates and bicarbonates can be generated by the equilibrium between the CO_2 and OH^- ions.[31]

$$\text{Dry electrolyte } 2CO_2 + 2e^- \leftrightarrow CO + CO_3^{2-} \quad (1)$$

$$\text{Water-containing electrolytes } CO_2 + H_2O + 2e^- \leftrightarrow CO + 2OH^- \quad (2)$$

$$CO_2 + OH^- \leftrightarrow HCO_3^- \quad (3)$$

$$HCO_3^- + OH^- \leftrightarrow CO_3^{2-} + H_2O \quad (4)$$

Due to their widespread use as nonaqueous electrolytes for CO_2RR, quaternary ammonium salts should form soluble carbonate species in organic solvents. To further probe this hypothesis, we generated different inorganic carbonate species in DME by bubbling CO_2 in solutions containing NaOH and TBAOH. As shown in Figure S7, the sample containing NaOH forms a white precipitate upon the introduction of CO_2, while

Table 1. Summary of Potential Glyme Ether Solvents and DMSO for CO_2RR, Their Solvent Properties, and CO_2 Solubility Values

solvent		CO_2 solubility (mmol/L)	permittivity at 25 °C	viscosity [mm^2/s]	DN [$kcal.mol^{-1}$]	AN
1,2-dimethoxyethane	(DME)	227 ± 15[a]	7.07[65]	0.5[49]	20[66]	10.2[66]
diglyme	(DGME)	160 ± 8.3[a]	7.63[65]	1.2[49]	18[66]	9.9[66]
tetraglyme	(TGME)	127 ± 6.3[a]	7.78[65]	4.1[49]	12[36,67]	10.5[36,67]
dimethyl sulfoxide	(DMSO)	130 ± 7[68]	46.7	2.0[69]	29.8	19.3

[a]Determined experimentally in this work (further details in the Supporting Information).

https://doi.org/10.1021/acs.jpcc.2c03321
J. Phys. Chem. C 2022, 126, 13595−13606

the TBAOH solution does not. Hence, TBA salts were chosen to serve as supporting ions to further investigate the influence of the solvent and counterion on the CO_2RR performance.

Despite their good reductive stability and high CO_2 solubility, glyme ether solvents impose new challenges to the electrochemical reduction of CO_2. As shown in Table 1, all glyme ethers have low acceptor number (AN), low donor number (DN), and low dielectric constants, which may result in poor salt solubility and low ionic conductivity. Moreover, the increase in the ether chain length results in a significant increase in the dynamic viscosity, which may affect charge mobility and electron transfer rates.[64]

To understand the effect of the solvent properties on the CO_2RR performance, linear sweep voltammetry experiments were first performed at Cu electrodes in 0.5 M TBAOTf in different glyme ether solvents (DME, DGME, and TGME). The corresponding voltammograms (LSVs) are presented in Figure 2a. When CO_2 is present, negative reductive currents

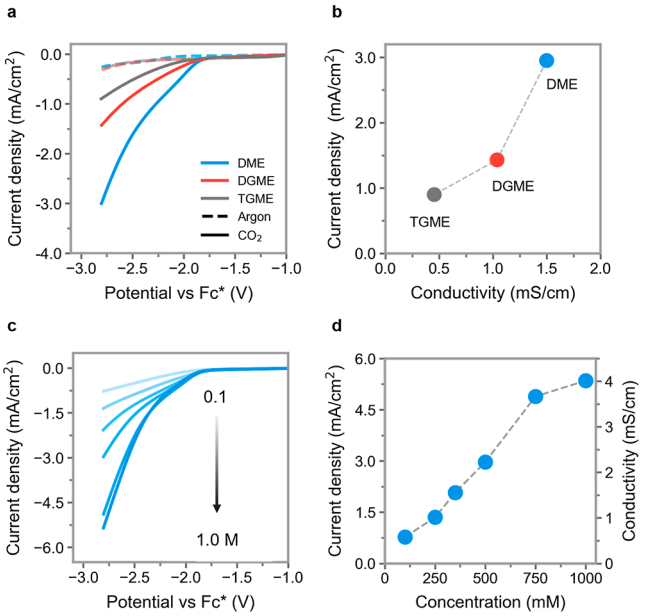

Figure 2. Influence of glyme ethers. (**a**) LSVs for Cu electrode at 50 mV/s in an argon atmosphere (dashed line) and CO_2 atmosphere (solid lines) in 0.5 M TBAOTf in different glyme ethers. (**b**) Ionic conductivity of different glyme ether solutions containing 0.5 M TBAOTf vs current density extracted from the respective voltammograms (in **a**) at −2.8 V vs Fc*. (**c**) LSVs for Cu electrode at 50 mV/s in CO_2 atmosphere at different salt concentrations (0.1, 0.2, 0.3, 0.5, 0.75, and 1.0 M) of TBAOTf in DME. (**d**) Conductivity of solutions containing different TBAOTf concentrations in DME vs current density extracted from the respective voltammograms (in **c**) at −2.8 V vs Fc*.

are observed, starting around −1.8 V for all three glyme ethers, which is commonly attributed to the formation of the $CO_2^{\bullet-}$ radical[62,70] in aprotic media. On the other hand, an increase in the alkoxy chain length (moving from DME to TGME) resulted in a decrease in the CO_2RR current density. This result can be correlated to a decrease in solution conductivity (Figure 2b), thus indicating that the solvent viscosity may also play a role in dictating the overall CO_2RR performance.

To understand the interplay between solution conductivity and CO_2RR current density, we performed experiments at different salt concentrations. As shown in Figure 2c, the increase in salt concentration up to 750 mM results in a significant increase in CO_2RR current density in DME. The increase in salt concentration also leads to an increase in solution conductivity (Figure 2d). However, above 750 mM, the increase in current density with salt concentration is less pronounced, most likely because the solution becomes visually more viscous. Therefore, we developed our subsequent studies of CO_2RR in DME at a salt concentration of 500 mM.

Electrolyte Effects on CO_2RR Current Densities. It has been widely reported that the solvation structure of different cationic species in an aqueous medium can directly affect the CO_2RR current density and product distribution.[22−24] However, these studies did not consider the competing formation of ion pairs, which are more commonly observed in nonaqueous solvents due to their poor ability to solvate ionic species compared to water.[37] In general, the equilibrium between the ionic species in solution can be written as $C_{(Sol)} + A_{(Sol)} \rightleftharpoons (C - A)_{(Sol)}$, where C and A represent the cation and anion, respectively, and Sol represents the solvated state. The quaternary ammonium cations used in this work are usually poorly solvated due to the steric hindrance generated by the alkyl groups. Moreover, glyme ethers weakly coordinate with anionic species due to their low dielectric constant and low AN (acceptor number) values,[34] as shown in Table 1. Therefore, the combined characteristics of glyme ethers and TBA salts can significantly shift the ionic equilibrium to the right, thereby enhancing the role of the anion in the formation of ion pairs.

Figure 3 shows LSVs for five different TBA salts. TBA salts containing halides (I^-, Cl^-, and F^-), PF_6^-, and acetate were poorly soluble in DME. As Figure 3a shows, all TBA salts present a significant increase in the cathodic current around −1.8 V versus Fc* at the Cu electrode in DME. However, the anion nature had a significant effect on the CO_2RR current density. Electrolytes containing OTf^- and $TFSI^-$ can reach current density values around 3 mA/cm^2 and beyond. However, electrolytes containing BF_4^-, ClO_4^-, and NO_3^- presented values below 1.5 mA/cm^2. Unlike the previous work,[31] we could not ascribe these differences in current density to the differences in the electrolyte water content because it was kept below 60 ppm for all TBA solutions over the LSV experiments (see the water content of the pure solvents and TBA solutions in Tables S1 and S2, respectively). Although we acknowledge that small amounts of water can affect the CO_2RR electrochemistry, the trends in current density among the TBA solutions do not correlate to the minor differences in water content.

To decouple the differences observed in the electrochemical behavior of the TBA salts from any catalyst modification, we further investigated the copper electrode surface after CO_2RR using XPS. Our XPS results (Figure S3) show no major differences for C 1s, Cu 2p, and O 1s for most electrolytes when compared to the pristine copper foil. We did not observe any significant deposition of Pt from the counter electrode to the working electrodes from the XPS survey spectra (Figure S4). However, for the electrolyte containing OTf anions, we observed small peaks in both C 1s and F 1s spectra assigned to C-F bonds. These peaks could originate from either salt breakdown or residual salt adsorbed to the electrode surface. Despite the OTf^- singular behavior, the overall trend in current density observed for different anions was further supported by experiments conducted using a gold electrode. As depicted in Figure 3b, OTf^- and $TFSI^-$ salts again presented higher current density values, with an increase in cathodic

https://doi.org/10.1021/acs.jpcc.2c03321
J. Phys. Chem. C 2022, 126, 13595−13606

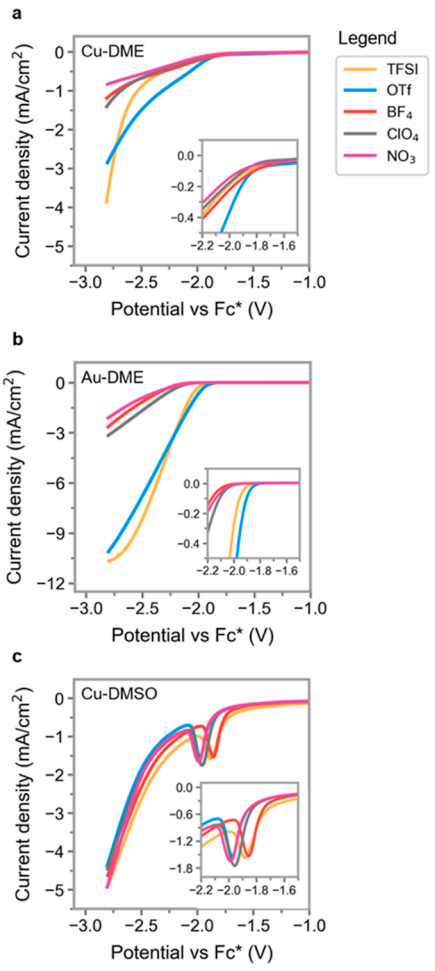

Figure 3. Catalyst and electrolyte effects. LSVs in CO_2 atmosphere in the presence of 0.5 M TBA salts at 50 mV/s for (**a**) Cu electrodes in DME, (**b**) Au electrodes in DME, and (**c**) Cu electrodes in DMSO.

current starting at potentials 0.2 V less negative than ClO_4^-, BF_4^-, and NO_3^- salts. As a noble metal, gold electrode is more stable than copper in the applied potential range in both aqueous and nonaqueous media.[71] Therefore, the influence of the anion appears the same across different catalysts (Cu and Au) and may not be attributed only to the catalyst surface changes.

In contrast to the observations in DME, experiments conducted in highly coordinating DMSO (Figure 3c) did not show any significance in cathodic current density across the different TBA salts. All DMSO electrolytes presented current density values significantly greater than those observed by the respective salts in DME. Despite the higher current density values observed for all TBA salts in DMSO and OTf^-/$TFSI^-$ salts in DME, it is important to highlight that those electrolytes also presented higher conductivity values when compared to the remaining ClO_4^-, BF_4^-, and NO_3^- salts. As discussed earlier, the solution conductivity in TBAOTf solutions can be directly correlated to the final product's current density. To decouple the solution conductivity from the anion effect on the CO_2RR current density, we performed LSV experiments with solutions containing different salt concentrations in DME. As shown in Figure S8, electrolytes containing 1200 mM NO_3^-, 500 mM ClO_4^-, and 350 mM OTf present similar conductivity values at around 1.5 mS/cm. However, they still present significant differences in current density, maintaining the previously observed trend where $OTf^- > ClO_4^- > NO_3^-$. We also observed similar behavior for solutions containing 750 mM ClO_4^- and 500 mM OTf^- that have similar ionic conductivities (2 mS/cm), but the OTf^- solutions led to higher current density values. As the anion effect in DME could not be ascribed to modifications on either the electrode surface or solution conductivity, we conducted a more detailed analysis of the electrolyte structure in the solution.

Ion Solvation Studies. The influence of salt and solvent selection on the ionic solvation structure was probed using spectroscopic techniques. We first investigated the structures of all electrolytes in DME using ^{1}H NMR (nuclear magnetic resonance) spectroscopy (see Figures S9 and S10). As the cation and solvent were kept constant across all salts, the differences in the ^{1}H chemical shifts from TBA^+ can only then be attributed to the differences in the interaction with the anion. Figure 4a illustrates how a TBA^+ cation can interact with an OTf^- anion through the more polarized hydrogens in the alpha position (α-H). Figure 4b,c shows the ^{1}H chemical shifts for all protons present in the TBA^+ cation in the presence of different anions in DME and DMSO, respectively. As expected, the α-H protons were the most susceptible to ion−dipole interactions as the anion is changed. This preference can be observed by the greater differences in the chemical shift for α-H among the anions in comparison to the protons in subsequent positions (β, λ, and δ) for both DME and DMSO.

As observed for other organic salts and ionic liquids, the chemical shift from the TBA^+ α-H can be correlated to the hydrogen-bond acceptance ability of the anion. The smaller and planar structure of nitrate anions makes them better hydrogen-bond acceptors,[72,73] resulting in a more downfield chemical shift for α-H from the TBA salts when compared to other anions. On the other hand, salts containing weakly coordinating anions, such as BF_4^-, OTf^-, and $TFSI^-$, presented a more upfield chemical shift. These differences in the chemical shift were more pronounced in the low dielectric constant DME than in DMSO, which presented a maximum α-H chemical shift gap across all TBA salts of 0.25 and 0.05 ppm, respectively. In general, the trends in the α-H chemical shift in DME, $TFSI^- < BF_4^- < OTf^- < ClO_4^- < NO_3^-$, followed an inverse relation with the CO_2RR current density. As an exception, the solution containing BF_4^- anions had a more downfield α-H chemical shift when compared to OTf^- and ClO_4^- solutions, while presenting smaller current density values than that of those anions. We also observed that all TBA salts in DMSO presented similar and more upfield chemical shifts than those in DME, while also presenting similar and higher values for current density.

We further investigated the TBA^+ solvation structures in DME and DMSO using electrospray ionization mass spectrometry (ESI-MS). By quantifying the relative abundance of all TBA^+-containing species, it is possible to map out the different ionic pairs within the TBA^+ solvation sheath. In general, ion pairs in the solution can be categorized into (i) contact ion pairs/aggregates, which involve the direct contact of two/multiple ionic species with opposite charges in solution and (ii) solvent-separated ion pairs, wherein the charged species are separated by one/multiple solvent molecules (illustration of different solvation structures is depicted in Figure S11). In the ESI-MS spectra illustrated in Figure 4d,e, we did not observe any solvent-separated ion pairs for all TBA salts for both DME and DMSO, respectively. These results indicate that TBA^+ does not interact strongly with the solvent,

https://doi.org/10.1021/acs.jpcc.2c03321
J. Phys. Chem. C 2022, 126, 13595−13606

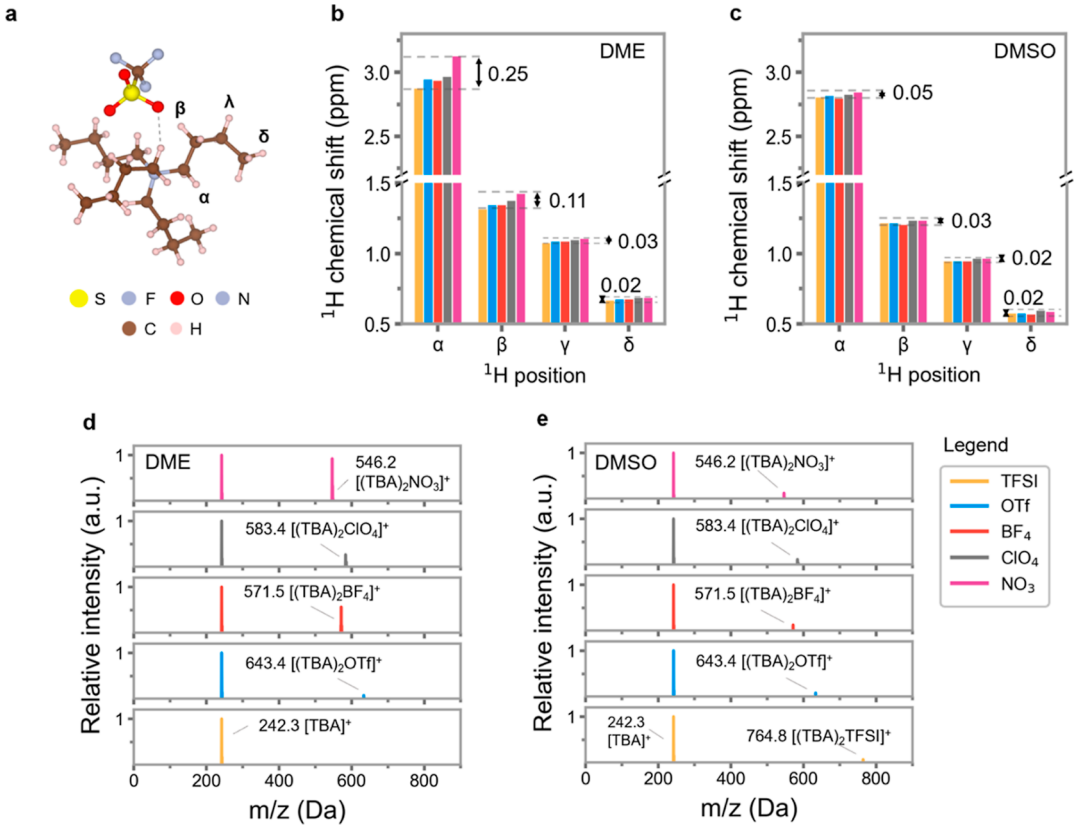

Figure 4. Ion solvation. (**a**) Illustration of TBA^+ cation interacting with an OTf^- anion and hydrogen labeling according to their relative position to the nitrogen atom in the TBA^+ structure. ^{1}H NMR chemical shift for 0.5 M TBA^+ salts in (**b**) DME and (**c**) DMSO, and ESI-MS spectra (positive mode) for different TBA^+ salts (0.5 M) in (**d**) DME and (**e**) DMSO. The abundance of the ion aggregates was normalized by the respective abundance of the free TBA^+ ions.

even with the highly coordinating DMSO. However, the population of ion aggregates (composed of two TBA^+ and one anion) was a function of both the solvent and anionic species.

The formation of ion aggregates can be attributed to the properties of both the solvent and supporting electrolyte. On the one hand, the solvent dielectric constant can be directly related to its ability to dissociate ions in solution,[37,73] which may explain the lower population of ion aggregates observed for TBA^+ salts in DMSO (Figure 4e). On the other hand, the alkyl groups in the TBA^+ structure hinder its interactions with larger anions, such as OTf^- and $TFSI^-$. This anion effect on the population of ion aggregates was observed in DME, where the ions are not easily dissociated due to the low dielectric constant (Figure 4d). Our spectroscopic observations in Figure 4 can now be directly related to the electrochemical measurements. As shown in Figure 5, while the fraction of ion aggregates increases in DME (moving from $TFSI^-/OTf^-$ to ClO_4^-, BF_4^-, and NO_3^-), the current density decreases. In contrast, all TBA^+ salts presented a low population of ion aggregates and large CO_2RR current density values when dissolved in DMSO. We also observed a similar trend for the TBA^+ α-H chemical shift, where a more upfield chemical shift can be correlated to larger current density values, not only across different salts in DME but also across different solvents. We probed the effect of the solvent dielectric constant on the salt dissociation and electrochemical properties by using density functional theory (DFT)[74] calculations, which show more negative complexation energy for all TBA salts in DME when compared to DMSO (Figure S12).

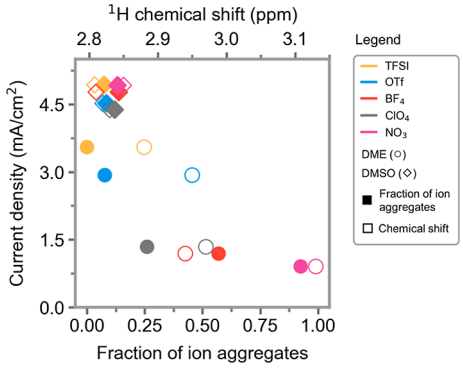

Figure 5. Solvation and electrochemistry correlation. Correlation between the current density extracted from the LSV plots (Figure 3a,c) at −2.8 V vs Fc* for Cu electrodes for different TBA salts in DME (circles) and DMSO (diamonds) vs (i) α-H chemical shifts from TBA^+ (hollow icons) extracted from ^{1}H NMR results (Figure 4b,c) and (ii) fraction of ion aggregates (solid icons) extracted from ESI-MS results (Figure 4d,e).

To further understand how the electrolyte bulk properties affect the CO_2RR performance at the electrode/electrolyte interface, we investigated the capacitance of the electrochemical double layer (C_{dl}) for different electrolytes in DME using a gold electrode. C_{dl} in the nonfaradaic region was investigated through cyclic voltammetry around the open-circuit potential at multiple scan rates (Figures S13 and S14). Electrochemical impedance spectroscopy (EIS) was used to investigate C_{dl} around −2.75 V versus Fc* by fitting the

https://doi.org/10.1021/acs.jpcc.2c03321
J. Phys. Chem. C 2022, 126, 13595−13606

experimental data to the simulation of the equivalent circuit depicted in Figure S15 (further description of the simulation and its parameters is provided in Figure S16 and Table S3). For the nonfaradaic region, we observed that C_{dl} values follow the same trend as that for the fraction of ion aggregates, with the electrolytes containing NO_3^- and BF_4^- salts reaching C_{dl} values close to 100 μF/cm^2 (Figure S14). These values are 3 to 4 times higher than the C_{dl} values found for OTf^- and $TFSI^-$ electrolytes. However, experiments in the nonfaradaic region cannot capture the drastic distortion of the ion arrangement in the electrochemical double layer and asymmetric ion movements at redox potentials, which can significantly affect the capacitance.[75]

Our C_{dl} studies in the faradaic region using EIS have revealed an opposite trend, where OTF^- and $TFSI^-$ electrolytes presented higher C_{dl} values than the remaining salts (Figure S17). A more compact electrochemical double layer can enhance the CO_2 reduction reaction by stabilizing high-dipole intermediates near the catalyst surface.[22−24] Since the seminal work developed by Amatore and Saveant,[63] the formation of $CO_2^{\bullet-}$ has been considered the rate-determining step for the CO_2RR in a low protic medium.[31,62,70] Our DFT calculations have then shown that TBA cations can interact with the negatively charged $CO_2^{\bullet-}$ through its α-hydrogens, with a binding enthalpy of −16.7 kcal/mol. Therefore, the stabilization of $CO_2^{\bullet-}$ by the larger population of free TBA^+ ions near that catalyst surface could explain the larger current densities observed for electrolytes with a lower population of ion aggregates, such as $TFSI^-$ and OTF^-. These observations are vital as we directly correlate the bulk solvation behavior (as observed in NMR and ESI-MS) to the electrochemical CO_2RR that occurs at the catalyst−electrolyte interface.

Electrolyte Effect on Product Distribution. The effect of different TBA electrolytes on the CO_2RR product distribution was investigated using an asymmetrical H-Cell setup (Figure S1b). The different TBA solutions in DME were used as a catholyte, while the anolyte chamber was filled with a 0.5 M $TBAClO_4$ DME solution containing 0.5 M water. The catholyte and anolyte chambers were separated by a Nafion N-117 proton exchange membrane (PEM). When water is not added to the anolyte solution, electrolyte decomposition takes place, leading to the appearance of a dark brown solution whose products could then react with the proton exchange membrane.[7] The addition of water also results in oxygen evolution as the dominant anodic reaction, ensuring a constant flow of protons to the cathodic chamber. The CO_2RR products in the gas and liquid phases were quantified using GC (gas chromatography) and ^{1}H NMR, respectively (further described in the Supporting Information).

Figure 6 summarizes the effect of the electrolyte and the applied potential on the CO_2RR product distribution for a Cu electrode. Herein, we only observed carbon monoxide, hydrogen, and formic acid as major CO_2RR products in DME. Our experiments conducted under an argon atmosphere (Figure S18) indicated that all products arise from CO_2RR rather than electrolyte/solvent decomposition. This product distribution is similar to what other authors have reported for Cu electrodes in nonaqueous electrolytes.[14,31] We also observed small amounts of methane at low overpotentials when TBAOTf was used as an electrolyte that can result from electrolyte decomposition (as seen with XPS data in Figure S3). We observed that both formic acid and methane production are electrode-dependent as none of these two products were formed for a gold working electrode (Figure S19).

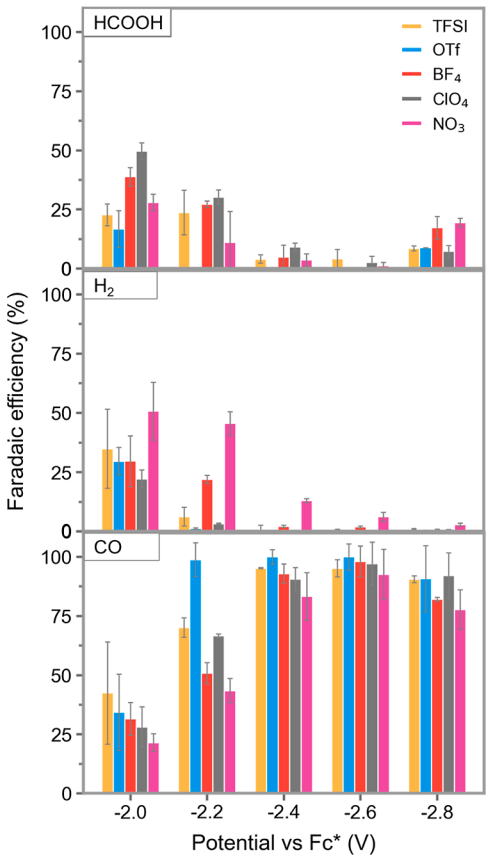

Figure 6. Electrolyte effect on CO_2RR product distribution. CO_2RR product distribution for different TBA salts (0.5 M) in DME as a catholyte and $TBAClO_4$ (0.5 M) containing 0.5 M of water in DME as an anolyte. A Cu disk (31.67 mm^2) was used as a cathode, a Ag/AgCl leakless electrode was used as a reference electrode, and Pt foil was used as an anode. FE values for the gaseous and liquid products were normalized to a total of 100%.

As a general trend, FE for CO increases with increasing overpotentials, reaching values above 90% at −2.6 V for all electrolytes and nearly 100% for OTf. The high FE values observed for CO for Cu electrodes in DME are comparable with those found for noble metal electrodes such as Au and Ag in both aqueous and nonaqueous electrolytes.[9,14,76] Interestingly, at potentials below −2.6 V, we found that OTf^- and $TFSI^-$ solutions presented similar or higher FE values for CO when compared to the remaining TBA salts. Hence, it appears that the solvation effects we discussed earlier not only modulate current densities but also CO_2RR product distributions, especially at lower reductive potentials. These differences in selectivity might be a result of the enhanced effect of the free cations on the stabilization of high-dipole intermediates that leads to the formation of CO (e.g., *CO).[22,23] On the other hand, we might expect a minor stabilizing effect on the formation of low-dipole intermediates that leads to the production of either formic acid or hydrogen (e.g., *OCHO, *COOH, and *H). This electrolyte effect in the CO_2RR selectivity can also be observed for experiments conducted in DMSO (Figure S20), where the low population of ion aggregates presented by both OTf^- and NO_3^- resulted in higher FE values for CO when compared to DME at the same potentials.

https://doi.org/10.1021/acs.jpcc.2c03321
J. Phys. Chem. C 2022, 126, 13595−13606

As HER is a competing reaction to CO_2RR, the FE values for hydrogen follow the opposite trend as for CO, reaching values close to zero as we moved to high overpotentials. Residual water in the electrolyte is most likely the main proton source for HER, and possible reasons for increased water content during the H-Cell experiments are further discussed in the Supporting Information. Previous studies have shown that even small amounts of water can interfere in the electrode−electrolyte interface and H_2O mass transport, enhancing both HER and CO_2RR.[77−79] Nevertheless, when investigating the current densities during the H-Cell measurements (Figure S21), we observed that OTf^- and $TFSI^-$ electrolytes present higher current densities at larger overpotentials than the other salts, even at water contents above 1000 ppm for all electrolytes (Table S2). This result indicates a similar trend to the one observed during the LSV experiments for different TBA salts, regardless of the differences in the sample water content and cell setup.

CONCLUSIONS

We investigated the effect of ion solvation on the CO_2 reduction reaction in aprotic solvents. Our voltammetric and XPS studies in DME showed that the presence of alkali cations can suppress CO_2RR by forming an insulating carbonate layer that prevents any further electrochemical reaction at the catalyst surface. In contrast, most TBA salts were able to sustain CO_2RR at potentials down to −2.8 V versus Fc* without any apparent decomposition. We also observed that the effect of the anion on the CO_2RR current density is strongly affected by the nature of the solvent. For the low-coordinating DME solvent, $TFSI^-$ and OTf^- salts presented larger CO_2RR current density values when compared to BF_4^-, ClO_4^-, and NO_3^- salts. These results could not be ascribed only to the differences either in solution conductivity, water content, or catalyst surface modifications. On the contrary, the same TBA salts when dissolved in the highly coordinating DMSO presented similar current density values. Importantly, our spectroscopic studies showed that the CO_2RR current density values in aprotic solvents could be correlated to the differences in the electrolyte solvation structure. ^1H NMR experiments indicated that a more upfield chemical shift in α-H from TBA results in larger CO_2RR current density values, while ESI-MS measurements mirrored the NMR results by showing that an increase in current density is inversely related to the population of ion aggregates in solution. These correlations could be observed not only across different solvents but also across different anions in DME. The solvent's low dielectric constant prevents complete dissociation of the TBA salt, therefore enhancing the anion effect on the formation of ion pairs. Finally, we observed that a lower population of ion aggregates can also be correlated to higher FE values for CO and lower FE values for H_2 at lower overpotentials. Our findings show the impact of the solvation behavior, such as the population of ion aggregates, in dictating the CO_2RR product distribution and current density in different aprotic solvents relevant for integrated CO_2 capture and conversion.

ASSOCIATED CONTENT

Supporting Information

The Supporting Information is available free of charge at https://pubs.acs.org/doi/10.1021/acs.jpcc.2c03321.

Additional data and futher description of the methods used for the determination of CO_2 solubility, voltammetry, XPS, ^1H NMR, and GC studies, Karl-Fisher titration, C_{dl} determination, and computational details (PDF)

AUTHOR INFORMATION

Corresponding Author

Chibueze V. Amanchukwu − *Pritzker School of Molecular Engineering, The University of Chicago, Chicago, Illinois 60637, United States;* orcid.org/0000-0002-6573-1213; Email: chibueze@uchicago.edu

Authors

Reginaldo J. Gomes − *Pritzker School of Molecular Engineering, The University of Chicago, Chicago, Illinois 60637, United States*

Chris Birch − *Pritzker School of Molecular Engineering, The University of Chicago, Chicago, Illinois 60637, United States*

Morgan M. Cencer − *Materials Science Division, Argonne National Laboratory, Lemont, Illinois 60439, United States;* orcid.org/0000-0003-2806-8317

Chenyang Li − *Materials Science Division, Argonne National Laboratory, Lemont, Illinois 60439, United States;* orcid.org/0000-0002-5155-4631

Seoung-Bum Son − *Chemical Sciences and Engineering Division, Argonne National Laboratory, Lemont, Illinois 60439, United States;* orcid.org/0000-0002-3723-6186

Ira D. Bloom − *Chemical Sciences and Engineering Division, Argonne National Laboratory, Lemont, Illinois 60439, United States;* orcid.org/0000-0002-4877-473X

Rajeev S. Assary − *Materials Science Division, Argonne National Laboratory, Lemont, Illinois 60439, United States;* orcid.org/0000-0002-9571-3307

Complete contact information is available at: https://pubs.acs.org/10.1021/acs.jpcc.2c03321

Notes

The authors declare no competing financial interest.

ACKNOWLEDGMENTS

This work was supported by the generous start-up funds from the University of Chicago, the Neubauer Family Assistant Professors program, and the University of Chicago Data Science Institute AI + Science seed funding. C.B. was supported by the UChicago Metcalf fellowship. NMR measurements were taken at the UChicago Chemistry NMR Facility, and XPS measurements were partly done at the UChicago Chemistry XPS Facility and Argonne National Laboratory. R.S.A. and C.L. would like to acknowledge Consortium for Computational Physics and Chemistry (CCPC), which is supported by the Bioenergy Technologies Office (BETO) of Energy Efficiency & Renewable Energy (EERE). Argonne National Laboratory is operated for DOE Office of Science by UChicago Argonne, LLC, under contract number DE-AC02-06CH11357. The authors thank Alexander Filatov for performing part of the XPS experiments presented in this work. The U.S. government retains for itself, and others acting on its behalf, a paid-up nonexclusive, irrevocable worldwide license in said article to reproduce, prepare derivative works, distribute copies to the public, and perform

publicly and display publicly, by or on behalf of the government.

REFERENCES

(1) Chen, A.; Lin, B.-L. A Simple Framework for Quantifying Electrochemical CO2 Fixation. *Joule* **2018**, *2*, 594−606.
(2) De Luna, P.; Hahn, C.; Higgins, D.; Jaffer, S. A.; Jaramillo, T. F.; Sargent, E. H. What Would It Take for Renewably Powered Electrosynthesis to Displace Petrochemical Processes? *Science* **2019**, *364*, 364eaav3506.
(3) Shin, H.; Hansen, K. U.; Jiao, F. Techno-Economic Assessment of Low-Temperature Carbon Dioxide Electrolysis. *Nat. Sustain.* **2021**, *4*, 911−919.
(4) Somoza-Tornos, A.; Guerra, O. J.; Crow, A. M.; Smith, W. A.; Hodge, B.-M. Process Modeling, Techno-Economic Assessment, and Life Cycle Assessment of the Electrochemical Reduction of CO2: A Review. *Iscience* **2021**, *24*, 102813.
(5) Birdja, Y. Y.; Pérez-Gallent, E.; Figueiredo, M. C.; Göttle, A. J.; Calle-Vallejo, F.; Koper, M. T. M. Advances and Challenges in Understanding the Electrocatalytic Conversion of Carbon Dioxide to Fuels. *Nat. Energy* **2019**, *4*, 732−745.
(6) Bagger, A.; Ju, W.; Varela, A. S.; Strasser, P.; Rossmeisl, J. Electrochemical CO2 Reduction: A Classification Problem. *ChemPhysChem* **2017**, *18*, 3266−3273.
(7) Ting, L. R. L.; García-Muelas, R.; Martín, A. J.; Veenstra, F. L. P.; Chen, S. T.-J.; Peng, Y.; Per, E. Y. X.; Pablo-García, S.; López, N.; Pérez-Ramírez, J.; et al. Electrochemical Reduction of Carbon Dioxide to 1-Butanol on Oxide-Derived Copper. *Angew. Chem., Int. Ed.* **2020**, *59*, 21072−21079.
(8) Ooka, H.; Figueiredo, M. C.; Koper, M. T. M. Competition between Hydrogen Evolution and Carbon Dioxide Reduction on Copper Electrodes in Mildly Acidic Media. *Langmuir* **2017**, *33*, 9307−9313.
(9) Goyal, A.; Marcandalli, G.; Mints, V. A.; Koper, M. T. M. Competition between CO2 Reduction and Hydrogen Evolution on a Gold Electrode under Well-Defined Mass Transport Conditions. *J. Am. Chem. Soc.* **2020**, *142*, 4154−4161.
(10) Rabinowitz, J. A.; Kanan, M. W. The Future of Low-Temperature Carbon Dioxide Electrolysis Depends on Solving One Basic Problem. *Nat. Commun.* **2020**, *11*, 5231.
(11) Dinh, C. T.; Burdyny, T.; Kibria, G.; Seifitokaldani, A.; Gabardo, C. M.; García de Arquer, F.; Kiani, A.; Edwards, J. P.; De Luna, P.; Bushuyev, O. S.; et al. CO2 Electroreduction to Ethylene via Hydroxide-Mediated Copper Catalysis at an Abrupt Interface. *Science* **20182018**, *360*, 783−787.
(12) Amanchukwu, C. v. The Electrolyte Frontier: A Manifesto. *Joule* **2020**, *4*, 281−285.
(13) Medina-Ramos, J.; DiMeglio, J. L.; Rosenthal, J. Efficient Reduction of CO2 to CO with High Current Density Using in Situ or Ex Situ Prepared Bi-Based Materials. *J. Am. Chem. Soc.* **2014**, *136*, 8361−8367.
(14) Ikeda, S.; Takagi, T.; Ito, K. Selective Formation of Formic Acid, Oxalic Acid, and Carbon Monoxide by Electrochemical Reduction of Carbon Dioxide. *Bull. Chem. Soc. Jpn.* **1987**, *60*, 2517−2522.
(15) Tomita, Y.; Hori, Y. Electrochemical Reduction of Carbon Dioxide at a Platinum Electrode in Acetonitrile-Water Mixtures. In *Advances in Chemical Conversions for Mitigating Carbon Dioxide*; Inui, T., Anpo, M., Izui, K., Yanagida, S., Yamaguchi, T. B. T.-S., Eds.; Elsevier, 1998; Vol. *114*, pp 581−584.
(16) Zhu, Q.; Ma, J.; Kang, X.; Sun, X.; Liu, H.; Hu, J.; Liu, Z.; Han, B. Efficient Reduction of CO2 into Formic Acid on a Lead or Tin Electrode Using an Ionic Liquid Catholyte Mixture. *Angew. Chem., Int. Ed.* **2016**, *55*, 9012−9016.
(17) Fischer, J.; Lehmann, T.; Heitz, E. The Production of Oxalic Acid from CO 2 and H 2 O. *J. Appl. Electrochem.* **1981**, *11*, 743−750.
(18) König, M.; Vaes, J.; Klemm, E.; Pant, D. Solvents and Supporting Electrolytes in the Electrocatalytic Reduction of CO2. *iScience* **2019**, *19*, 135−160.
(19) Gennaro, A.; Isse, A. A.; Vianello, E. Solubility and Electrochemical Determination of CO2 in Some Dipolar Aprotic Solvents. *J. Electroanal. Chem.* **1990**, *289*, 203−215.
(20) Bucklin, R. W.; Schendel, R. L. Comparison of Fluor Solvent and Selexol Processes. *Environ. Prog.* **1984**, *4*, 137−142.
(21) Burr, B.; Lyddon, L. *A Comparison of Physical Solvents for Acid Gas Removal*; Bryan Research & Engineering. Inc.: Bryan, Texas, USA, 2008.
(22) Ringe, S.; Clark, E. L.; Resasco, J.; Walton, A.; Seger, B.; Bell, A. T.; Chan, K. Understanding Cation Effects in Electrochemical CO2 Reduction. *Energy Environ. Sci.* **2019**, *12*, 3001−3014.
(23) Resasco, J.; Chen, L. D.; Clark, E.; Tsai, C.; Hahn, C.; Jaramillo, T. F.; Chan, K.; Bell, A. T. Promoter Effects of Alkali Metal Cations on the Electrochemical Reduction of Carbon Dioxide. *J. Am. Chem. Soc.* **2017**, *139*, 11277−11287.
(24) Monteiro, M. C. O.; Dattila, F.; Hagedoorn, B.; García-Muelas, R.; López, N.; Koper, M. T. M. Absence of CO2 Electroreduction on Copper, Gold and Silver Electrodes without Metal Cations in Solution. *Nat. Catal.* **2021**, *4*, 654−662.
(25) Wuttig, A.; Yoon, Y.; Ryu, J.; Surendranath, Y. Bicarbonate Is Not a General Acid in Au-Catalyzed CO2 Electroreduction. *J. Am. Chem. Soc.* **2017**, *139*, 17109−17113.
(26) Resasco, J.; Lum, Y.; Clark, E.; Zeledon, J. Z.; Bell, A. T. Effects of Anion Identity and Concentration on Electrochemical Reduction of CO2. *ChemElectroChem* **2018**, *5*, 1064−1072.
(27) Gao, D.; Scholten, F.; Roldan Cuenya, B. Improved CO2 Electroreduction Performance on Plasma-Activated Cu Catalysts via Electrolyte Design: Halide Effect. *ACS Catal.* **2017**, *7*, 5112−5120.
(28) Huang, Y.; Ong, C. W.; Yeo, B. S. Effects of Electrolyte Anions on the Reduction of Carbon Dioxide to Ethylene and Ethanol on Copper 100) and 111) Surfaces. *ChemSusChem* **2018**, *11*, 3299−3306.
(29) Berto, T. C.; Zhang, L.; Hamers, R. J.; Berry, J. F. Electrolyte Dependence of CO2 Electroreduction: Tetraalkylammonium Ions Are Not Electrocatalysts. *ACS Catal.* **2015**, *5*, 703−707.
(30) Niu, D.; Wang, H.; Li, H.; Zhang, X. The Effect of the Alkyl Chain Length of the Tetraalkylammonium Cation on CO2 Electroreduction in an Aprotic Medium. *Electrochem. Commun.* **2015**, *52*, 58−62.
(31) Figueiredo, M. C.; Ledezma-Yanez, I.; Koper, M. T. M. In Situ Spectroscopic Study of CO2 Electroreduction at Copper Electrodes in Acetonitrile. *ACS Catal.* **2016**, *6*, 2382−2392.
(32) Amanchukwu, C. v.; Chang, H.-H.; Hammond, P. T. Influence of Ammonium Salts on Discharge and Charge of Li−O2 Batteries. *J. Phys. Chem. C* **2017**, *121*, 17671−17681.
(33) Amanchukwu, C. v.; Chang, H.-H.; Gauthier, M.; Feng, S.; Batcho, T. P.; Hammond, P. T. One-Electron Mechanism in a Gel−Polymer Electrolyte Li−O2 Battery. *Chem. Mater.* **2016**, *28*, 7167−7177.
(34) Lutz, L.; Alves Dalla Corte, D.; Tang, M.; Salager, E.; Deschamps, M.; Grimaud, A.; Johnson, L.; Bruce, P. G.; Tarascon, J.-M. Role of Electrolyte Anions in the Na−O2 Battery: Implications for NaO2 Solvation and the Stability of the Sodium Solid Electrolyte Interphase in Glyme Ethers. *Chem. Mater.* **2017**, *29*, 6066−6075.
(35) Johnson, L.; Li, C.; Liu, Z.; Chen, Y.; Freunberger, S. A.; Ashok, P. C.; Praveen, B. B.; Dholakia, K.; Tarascon, J.-M.; Bruce, P. G. The Role of LiO 2 Solubility in O 2 Reduction in Aprotic Solvents and Its Consequences for Li−O 2 Batteries. *Nat. Chem.* **2014**, *6*, 1091−1099.
(36) Lutz, L.; Yin, W.; Grimaud, A.; Alves Dalla Corte, D.; Tang, M.; Johnson, L.; Azaceta, E.; Sarou-Kanian, V.; Naylor, A. J.; Hamad, S.; et al. High Capacity Na−O2 Batteries: Key Parameters for Solution-Mediated Discharge. *J. Phys. Chem. C* **2016**, *120*, 20068−20076.
(37) Giesecke, M.; Mériguet, G.; Hallberg, F.; Fang, Y.; Stilbs, P.; Furó, I. Ion Association in Aqueous and Non-Aqueous Solutions Probed by Diffusion and Electrophoretic NMR. *Phys. Chem. Chem. Phys.* **2015**, *17*, 3402−3408.
(38) Sharon, D.; Hirsberg, D.; Salama, M.; Afri, M.; Frimer, A. A.; Noked, M.; Kwak, W.; Sun, Y.-K.; Aurbach, D. Mechanistic Role of Li

https://doi.org/10.1021/acs.jpcc.2c03321
J. Phys. Chem. C 2022, 126, 13595−13606

+ Dissociation Level in Aprotic Li−O2 Battery. *ACS Appl. Mater. Interfaces* **2016**, *8*, 5300−5307.
(39) Ma, P.; Mirmira, P.; Amanchukwu, C. v. Effect of Building Block Connectivity and Ion Solvation on Electrochemical Stability and Ionic Conductivity in Novel Fluoroether Electrolytes. *ACS Cent. Sci.* **2021**, *7*, 1232−1244.
(40) Amanchukwu, C. v.; Kong, X.; Qin, J.; Cui, Y.; Bao, Z. Nonpolar Alkanes Modify Lithium-Ion Solvation for Improved Lithium Deposition and Stripping. *Adv. Energy Mater.* **2019**, *9*, 1902116.
(41) Freunberger, S. A.; Chen, Y.; Drewett, N. E.; Hardwick, L. J.; Bardé, F.; Bruce, P. G. The Lithium−Oxygen Battery with Ether-Based Electrolytes. *Angew. Chem., Int. Ed.* **2011**, *50*, 8609−8613.
(42) Black, R.; Shyamsunder, A.; Adeli, P.; Kundu, D.; Murphy, G. K.; Nazar, L. F. The Nature and Impact of Side Reactions in Glyme-Based Sodium−Oxygen Batteries. *ChemSusChem* **2016**, *9*, 1795−1803.
(43) Factor Analysis in Chemistry, 3rd Ed. Malinowski, E. R., Eds.; Wiley, New York, 2002, ISBN 0-471-13479-1, € 117.60, 2002, *16* 12), 635.
(44) Dietz Rago, N.; Bareño, J.; Li, J.; Du, Z.; Wood, D. L.; Steele, L. A.; Lamb, J.; Spangler, S.; Grosso, C.; Fenton, K.; et al. Effect of Overcharge on LiNi0.5Mn0.3Co0.2)O2/Graphite Lithium Ion Cells with PolyVinylidene Fluoride) Binder. I - Microstructural Changes in the Anode. *J. Power Sources* **2018**, *385*, 148−155.
(45) Bloom, I.; Bareño, J.; Dietz Rago, N.; Dogan, F.; Graczyk, D. G.; Tsai, Y.; Naik, S. R.; Han, S.-D.; Lee, E.; Du, Z.; et al. Effect of Overcharge on LiNi0.5Mn0.3Co0.2)O2 Cathodes: NMP-Soluble Binder. II — Chemical Changes in the Anode. *J. Power Sources* **2018**, *385*, 156−164.
(46) Fairley, N.; Fernandez, V.; Richard-Plouet, M.; Guillot-Deudon, C.; Walton, J.; Smith, E.; Flahaut, D.; Greiner, M.; Biesinger, M.; Tougaard, S.; et al. Systematic and Collaborative Approach to Problem Solving Using X-Ray Photoelectron Spectroscopy. *Appl. Surf. Sci.Adv.* **2021**, *5*, 100112.
(47) Choi, N.-S.; Chen, Z.; Freunberger, S. A.; Ji, X.; Sun, Y.-K.; Amine, K.; Yushin, G.; Nazar, L. F.; Cho, J.; Bruce, P. G. Challenges Facing Lithium Batteries and Electrical Double-Layer Capacitors. *Angew. Chem., Int. Ed.* **2012**, *51*, 9994−10024.
(48) Hobold, G. M.; Lopez, J.; Guo, R.; Minafra, N.; Banerjee, A.; Shirley Meng, Y.; Shao-Horn, Y.; Gallant, B. M. Moving beyond 99.9% Coulombic Efficiency for Lithium Anodes in Liquid Electrolytes. *Nat. Energy* **2021**, *6*, 951−960.
(49) Jache, B.; Binder, J. O.; Abe, T.; Adelhelm, P. A Comparative Study on the Impact of Different Glymes and Their Derivatives as Electrolyte Solvents for Graphite Co-Intercalation Electrodes in Lithium-Ion and Sodium-Ion Batteries. *Phys. Chem. Chem. Phys.* **2016**, *18*, 14299−14316.
(50) Ruther, R. E.; Yang, G.; Delnick, F. M.; Tang, Z.; Lehmann, M. L.; Saito, T.; Meng, Y.; Zawodzinski, T. A.; Nanda, J. Mechanically Robust, Sodium-Ion Conducting Membranes for Nonaqueous Redox Flow Batteries. *ACS Energy Lett.* **2018**, *3*, 1640−1647.
(51) Murata, A.; Hori, Y. Product Selectivity Affected by Cationic Species in Electrochemical Reduction of CO2 and CO at a Cu Electrode. **1991**, *64*(), 123−127. DOI: 10.1246/BCSJ.64.123.
(52) Li, J.; Wu, D.; Malkani, A. S.; Chang, X.; Cheng, M.-J.; Xu, B.; Lu, Q. Hydroxide Is Not a Promoter of C2+ Product Formation in the Electrochemical Reduction of CO on Copper. *Angew. Chem., Int. Ed.* **2020**, *59*, 4464−4469.
(53) Monteiro, M. C. O.; Dattila, F.; López, N.; Koper, M. T. M. The Role of Cation Acidity on the Competition between Hydrogen Evolution and CO2Reduction on Gold Electrodes. *J. Am. Chem. Soc.* **2022**, *144*, 1589−1602.
(54) Banerjee, S.; Han, X.; Thoi, V. S. Modulating the Electrode−Electrolyte Interface with Cationic Surfactants in Carbon Dioxide Reduction. *ACS Catal.* **2019**, *9*, 5631−5637.
(55) Kuhl, K. P.; Cave, E. R.; Abram, D. N.; Jaramillo, T. F. New Insights into the Electrochemical Reduction of Carbon Dioxide on Metallic Copper Surfaces. *Energy Environ. Sci.* **2012**, *5*, 7050−7059.
(56) Hatsukade, T.; Kuhl, K. P.; Cave, E. R.; Abram, D. N.; Jaramillo, T. F. Insights into the Electrocatalytic Reduction of CO2 on Metallic Silver Surfaces. *Phys. Chem. Chem. Phys.* **2014**, *16*, 13814−13819.
(57) Noviandri, I.; Brown, K. N.; Fleming, D. S.; Gulyas, P. T.; Lay, P. A.; Masters, A. F.; Phillips, L. The Decamethylferrocenium/Decamethylferrocene Redox Couple: A Superior Redox Standard to the Ferrocenium/Ferrocene Redox Couple for Studying Solvent Effects on the Thermodynamics of Electron Transfer. *J. Phys. Chem. B* **1999**, *103*, 6713−6722.
(58) Kwabi, D. G.; Bryantsev, V. S.; Batcho, T. P.; Itkis, D. M.; Thompson, C. v.; Shao-Horn, Y. Experimental and Computational Analysis of the Solvent-Dependent O2/Li+-O2− Redox Couple: Standard Potentials, Coupling Strength, and Implications for Lithium−Oxygen Batteries. *Angew. Chem., Int. Ed.* **2016**, *55*, 3129−3134.
(59) Setterfield-Price, B. M.; Dryfe, R. A. W. The Influence of Electrolyte Identity upon the Electro-Reduction of CO2. *J. Electroanal. Chem.* **2014**, *730*, 48−58.
(60) Xie, Z.; Zhang, X.; Zhang, Z.; Zhou, Z. Metal−CO2 Batteries on the Road: CO2 from Contamination Gas to Energy Source. *Adv. Mater.* **2017**, *29*, 1605891.
(61) Xu, S.; Lau, S.; Archer, L. A. CO2 and Ambient Air in Metal−Oxygen Batteries: Steps towards Reality. *Inorg. Chem. Front.* **2015**, *2*, 1070−1079.
(62) Gennaro, A.; Isse, A. A.; Severin, M.-G.; Vianello, E.; Bhugun, I.; Savéant, J.-M. Mechanism of the Electrochemical Reduction of Carbon Dioxide at Inert Electrodes in Media of Low Proton Availability. *J. Chem. Soc., Faraday Trans.* **1996**, *92*, 3963−3968.
(63) Amatore, C.; Saveant, J. M. Mechanism and Kinetic Characteristics of the Electrochemical Reduction of Carbon Dioxide in Media of Low Proton Availability. *J. Am. Chem. Soc.* **1981**, *103*, 5021−5023.
(64) Zhang, X.; Yang, H.; Bard, A. J. Variation of the Heterogeneous Electron-Transfer Rate Constant with Solution Viscosity: Reduction of Aqueous Solutions of [EDTA)ChromiumIII)]- at a Mercury Electrode. *J. Am. Chem. Soc.* **1987**, *109*, 1916−1920.
(65) Riadigos, C. F.; Iglesias, R.; Rivas, M. A.; Iglesias, T. P. Permittivity and Density of the Systems Monoglyme, Diglyme, Triglyme, or Tetraglyme+n-Heptane) at Several Temperatures. *J. Chem. Therm.* **2011**, *43*, 275−283.
(66) Schmid, R. Re-Interpretation of the Solvent Dielectric Constant in Coordination Chemical Terms. *J. Solution Chem.* **1983**, *12*, 135−152.
(67) Black, J. J.; Dolan, A.; Harper, J. B.; Aldous, L. Kamlet−Taft Solvent Parameters, NMR Spectroscopic Analysis and Thermoelectrochemistry of Lithium−Glyme Solvate Ionic Liquids and Their Dilute Solutions. *Phys. Chem. Chem. Phys.* **2018**, *20*, 16558−16567.
(68) Welford, P. J.; Brookes, B. A.; Wadhawan, J. D.; McPeak, H. B.; Hahn, C. E. W.; Compton, R. G. The Electro-Reduction of Carbon Dioxide in Dimethyl Sulfoxide at Gold Microdisk Electrodes: Current | Voltage Waveshape Analysis. *J. Phys. Chem. B* **2001**, *105*, 5253−5261.
(69) LeBel, R. G.; Goring, D. A. I. Density, Viscosity, Refractive Index, and Hygroscopicity of Mixtures of Water and Dimethyl Sulfoxide. *J. Chem. Eng. Data* **1962**, *7*, 100−101.
(70) Matsubara, Y.; Grills, D. C.; Kuwahara, Y. Thermodynamic Aspects of Electrocatalytic CO2 Reduction in Acetonitrile and with an Ionic Liquid as Solvent or Electrolyte. *ACS Catal.* **2015**, *5*, 6440−6452.
(71) Shi, J.; Shen, F.; Shi, F.; Song, N.; Jia, Y.-J.; Hu, Y.-Q.; Li, Q.-Y.; Liu, J.; Chen, T.-Y.; Dai, Y.-N. Electrochemical Reduction of CO2 into CO in Tetrabutylammonium Perchlorate/Propylene Carbonate: Water Effects and Mechanism. *Electrochim. Acta* **2017**, *240*, 114−121.
(72) Huynh, H. V.; Lam, T. T.; Luong, H. T. T. Anion Influences on Reactivity and NMR Spectroscopic Features of NHC Precursors. *RSC Adv.* **2018**, *8*, 34960−34966.
(73) Pike, S. J.; Hutchinson, J. J.; Hunter, C. A. H-Bond Acceptor Parameters for Anions. *J. Am. Chem. Soc.* **2017**, *139*, 6700−6706.

(74) Kohn, W.; Sham, L. J. Self-Consistent Equations Including Exchange and Correlation Effects. *Phys. Rev.* **1965**, *140*, A1133−A1138.
(75) Schalenbach, M.; Durmus, Y. E.; Tempel, H.; Kungl, H.; Eichel, R. A. Double Layer Capacitances Analysed with Impedance Spectroscopy and Cyclic Voltammetry: Validity and Limits of the Constant Phase Element Parameterization. *Phys. Chem. Chem. Phys.* **2021**, *23*, 21097−21105.
(76) Lu, Q.; Rosen, J.; Zhou, Y.; Hutchings, G. S.; Kimmel, Y. C.; Chen, J. G.; Jiao, F. A Selective and Efficient Electrocatalyst for Carbon Dioxide Reduction. *Nat. Commun.* **2014**, *5*, 3242.
(77) Rudnev, A. V.; Zhumaev, U. E.; Kuzume, A.; Vesztergom, S.; Furrer, J.; Broekmann, P.; Wandlowski, T. The Promoting Effect of Water on the Electroreduction of CO2 in Acetonitrile. *Electrochim. Acta* **2016**, *189*, 38−44.
(78) Ledezma-Yanez, I.; Koper, M. T. M. Influence of Water on the Hydrogen Evolution Reaction on a Gold Electrode in Acetonitrile Solution. *J. Electroanal. Chem.* **2017**, *793*, 18−24.
(79) Joshi, P. B.; Karki, N.; Wilson, A. J. Electrocatalytic CO $_2$ Reduction in Acetonitrile Enhanced by the Local Environment and Mass Transport of H $_2$ O. *ACS Energy Lett.* **2022**, *7*, 602−609.

https://doi.org/10.1021/acs.jpcc.2c03321
J. Phys. Chem. C 2022, 126, 13595−13606